Arbitrary hybrid and higher-order Poincaré sphere beams generation by metasurfaces via a unified design framework

Chuang Sun[1], Hailong Pi[1], Kian Shen Kiang[1], Jun-Yu Ou[2,], and Jize Yan[1,] **

Chuang Sun (https://orcid.org/0000-0001-7024-1916), Hailong Pi (https://orcid.org/0000-0002-3209-5396), Kian Shen Kiang (https://orcid.org/0000-0002-7326-909X), Jize Yan (https://orcid.org/0000-0002-2886-2847)
School of Electronics and Computer Science, University of Southampton, Southampton SO17 1BJ, UK
E-mail: J.Yan@soton.ac.uk

Jun-Yu Ou (https://orcid.org/0000-0001-8028-6130)
School of Physics and Astronomy, University of Southampton, Southampton SO17 1BJ, UK
E-mail: bruce.ou@soton.ac.uk

Abstract. The unique phase profile and polarisation distribution of the vector vortex beam have been a subject of increasing interest in classical and quantum optics. The development of higher-order Poincaré sphere and hybrid-order Poincaré sphere has provided a systematic description of vector vortex beams. However, the generation of arbitrary vector vortex beams on a higher-order and a hybrid-order Poincaré sphere via a metasurface lacks a unified design framework, despite numerous reported approaches. This paper presents a novel, unified general design framework incorporating all design parameters (e.g., focal length, orders) of arbitrary higher-order Poincaré sphere and hybrid-order Poincaré sphere beams into a single equation. In proof-of-concept experiments, we experimentally demonstrated four metasurfaces to generate arbitrary beams on the 5th-order higher-order Poincaré sphere (non-focused and tightly-focused, NA 0.89), 0-2 order and 0-1 order hybrid-order Poincaré sphere. We showed higher-order Poincaré sphere beams' propagation and focusing properties, the super-resolution focusing characteristics of the 1st-order cylindrical vector vortex beams, and the different focusing properties of integer-order and fractional-order cylindrical vector vortex beams. The simplicity and feasibility of the proposed design framework make it a potential catalyst for arbitrary vector vortex beams using metasurfaces in applications of optical imaging, communication, and optical trapping.

Keywords: Metasurface, vector vortex beams, Poincaré sphere.

*****[1]Jun-Yu Ou**,** E-mail: bruce.ou@soton.ac.uk
*****[2]Jize Yan**,** E-mail: J.Yan@soton.ac.uk

1 Introduction

Structured light beams are attracting researchers' attention in many fields because of their powerful application potentials in classic and quantum fields ranging from laser communication, super-resolution imaging and lithography, and multi-dimensional optical manipulation [1-5]. Vector

vortex beam (VVB), as a special group of structured light beams, owns a spatially inhomogeneous state of polarisation (SOP) and phase profile on its cross-section, which makes it carry orbital angular momentum (OAM) and spin angular momentum (SAM) [6].

A theoretical framework named higher-order Poincaré sphere (HOPS) is developed to describe the VVB's total angular momentum and its evolution of SOP and phase profile, which provides researchers with great utility and convenience in studying the VVB [7]. The two poles of HOPS represent two scalar vortex beams with spatially homogenous SOP [i.e., left circular polarisation (LCP) and right circular polarisation (RCP)] and vortex phase profile, which possesses a SAM of $\sigma\hbar$ ($\sigma = \pm 1$) and an OAM of $l\hbar$ (l is the orders of a HOPS and the topological charge of a vortex beam) [6,7]. The equator of a HOPS represents a set of cylindrical vector beams that carry no angular momentum and is a widely used type of VVBs because of its super-resolution imaging and lithography capability [3, 4, 6].

Constrained by the identical angular momentum carried by the HOPS beams, their applicability remains limited to specific scenarios [8]. The hybrid-order Poincaré sphere (HyOPS) is developed to broaden the scope of HOPS to a more general form, where the left- and right-circular polarisation beams represented by the northern and southern poles have distinct topological charges ($|\ell_{LCP}| \neq |\ell_{RCP}|$). As a result, the total angular momentum carried by a HyOPS beam varies across its surface [9]. Conventionally, HOPS and HyOPS beams can be generated by introducing a bulky anisotropic crystal, q-plate, spiral phase plate, and SLM to an optical path [1, 4, 6]. For instance, the HOPS can be generated in a multicore fibre amplifier by shaping the seed laser beam via an SLM [9]. In addition, the SLM is also used for the generating the multidimensional structured light described by the SU (2) Poincaré sphere [10 – 13].

Based on the generalised Fresnel theorem and abrupt phase induced by a subwavelength meta-atom [14], the metasurface, which is composed of an array of sub-wavelength meta-atoms on a flat substrate, is capable of engineering incoming light's amplitude, phase, and polarisation [15-19]. Furthermore, metasurface is lightweight, low-cost, mass-production, scale-up, and capable of integrating with an on-chip light source (e.g., vertical-cavity surface-emitting laser) [20, 21]. Therefore, many design approaches are developed for generating and focusing the cylindrical vector beams, HOPS beams, and HyOPS beams [22 - 34]. Compared with the plasmonic-based metasurface, the all-dielectric metasurface attracts intensive attention because it can avoid ohmic losses and realize high manipulation efficiency. Its fabrication requires only single-step lithography and is CMOS-compatible [15]. Till now, there is no unified theoretical framework to design single-layer all-dielectric metasurfaces for controlled generating unfocused and focused VVBs on a HOPS or a HyOPS. In addition, the HOPS and HyOPS beams have not been experimentally generated by metasurfaces in the wavelength of 1550nm, while this wavelength plays an essential role in laser communication, biological imaging, and optical manipulation [21, 35].

This paper derived the target phase profiles from the fundamental definition for generating arbitrary non-focused/focused vector vortex beams on HOPS and HyOPS. Then, a unified design framework of an all-dielectric metasurface for generating non-focused/focused vector vortex beams on a HOPS and HyOPS was proposed in section 3, and the controlled generation principle of the arbitrary vector vortex beams over the HOPS and HyOPS was analyzed. In section 4, we designed, fabricated, and characterized four metasurface samples working in the wavelength of 1550nm to generate arbitrary vector vortex beams on the 5^{th} order HOPS (non-focused and tightly focused), 0-2^{nd} order HyOPS, and 0-1^{st} order HyOPS. The experimental results agreed well with

the theoretical expectation values, showcasing the unified design framework's feasibility and potential applications.

2. Phase profiles for generating HOPS and HyOPS beams

Figure 1 shows a fundamental Poincaré sphere (FPS) [Fig. 1(a)], a HOPS [Fig. 1(b)], and a HyOPS [Fig. 1(c)]. Arbitrary vector vortex beams on a HyOPS can be expressed as Eq. (1), where α is the azimuthal angle in the polar coordinate of the light beam's cross-section, $\tilde{A}_{LN} = A_{LN}e^{i(\varphi_{LN})}$ and $\tilde{A}_{RM} = A_{RM}e^{i(\varphi_{RM})}$ are the complex amplitudes of the LCP (i.e., $|L\rangle = \frac{\sqrt{2}}{2}\begin{bmatrix}1\\ i\end{bmatrix}$) vortex component with a topological charge of N and the RCP (i.e., $|R\rangle = \frac{\sqrt{2}}{2}\begin{bmatrix}1\\ -i\end{bmatrix}$) vortex component with a topological charge of M [8]. Note that the N should not be equal to M for the HyOPS beams.

$$U = A_{LN}e^{i(\varphi_{LN})}e^{i(N\alpha)}|L\rangle + A_{RM}e^{i(\varphi_{RM})}e^{i(M\alpha)}|R\rangle \tag{1}$$

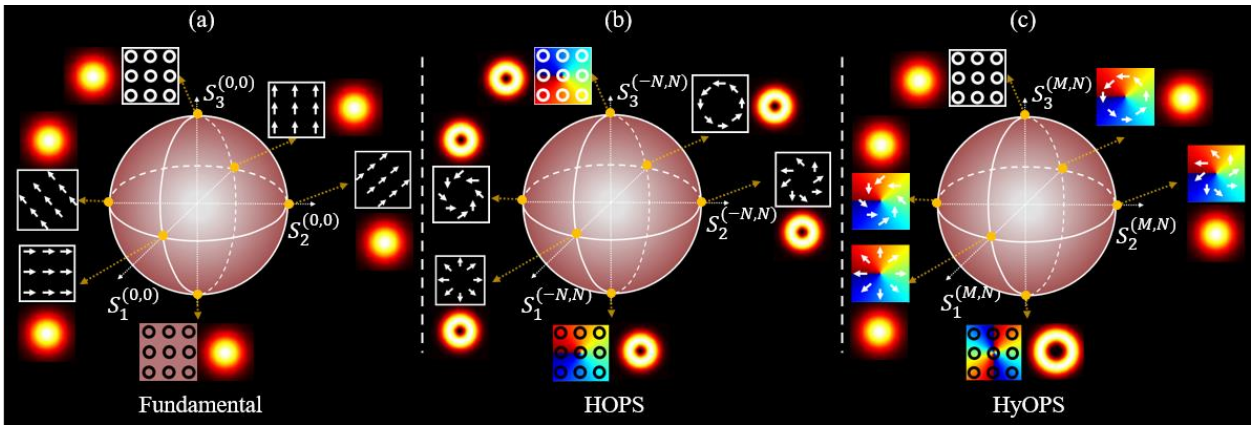

Fig. 1 (a) Fundamental Poincaré sphere, (b) HOPS, and (c) HyOPS. $S_1^{(N,M)}$, $S_2^{(N,M)}$, and $S_3^{(N,M)}$ are the Stokes parameters of the beams, and the superscript (M, N) denotes the topological charges carried by the LCP (southern pole) and RCP (northern pole) beams. When $M = -N$, the LCP and RCP beams are vortex beams of the same topological charge with opposite signs, and the HyOPS (c) is degraded to HOPS (b). Moreover, when $M = N = 0$, the LCP and RCP beams are plane waves, and the HOPS is degraded to a fundamental Poincaré sphere (a).

From Eq. (1), the vector vortex beams on a HyOPS combine two orthogonal LCP and RCP vortex components with different topological charges. As shown in Fig. 1(c), from the northern pole to the southern pole of a HyOPS, the Eq. (1) could vary from a scalar plane beam to a scalar vortex beam with a topologic charge of 2 by setting $M = 0$ and $N = 2$. The equator of the HyOPS represents a set of cylindrical vector vortex beams where the LCP and RCP components have the same amplitudes $A_{LN} = A_{RM}$.

The scalar beams on the FPS [Fig. 1(a)] have a uniform polarisation distribution overall in the beam's cross-section and Gaussian intensity distribution. When $N = M = 0$, Eq. (1) is simplified to Eq. (2), which describes all the scalar beams on the FPS. Therefore, the arbitrary polarisation state of a scalar beam can be decomposed into two orthogonal LCP and RCP components. The polarisation states would vary with the complex amplitudes $\tilde{A}_{LN}$ and $\tilde{A}_{RM}$. Specifically, the LCP and RCP components in a linear polarisation (LP) light beam have the same amplitudes $A_{LN} = A_{RM}$, and the phase difference $\Delta\varphi_{RL} = \varphi_{RM} - \varphi_{LN}$ determines the polarisation direction of an LP laser beam [7], illustrated by the FPS equator in Fig. 1(a). In experimental constructions, arbitrary scalar beams on an FPS can be obtained by combining a quarter waveplate (QWP) and half waveplate (HWP). In other words, the $\tilde{A}_{LN}$ and $\tilde{A}_{RM}$ can be easily tuned to arbitrary values via a QWP and a HWP.

$$U = \tilde{A}_{LN}|L\rangle + \tilde{A}_{RM}|R\rangle \tag{2}$$

As shown in Fig. 1(b), the light beams on a HOPS have a spatial-varied distribution in phase and polarisation. In addition, the orthogonal LCP and RCP components in an HOPS beam are vortex beams having the same topological charge *N* with opposite signs. Therefore, Eq. (1) can be rewritten into Eq. (3) for describing the HOPS beams by replacing *M* with -*N*. According to Fig. 1(b) and Eq. (3), the equator of a HOPS represents a set of cylindrical vector beams with an

order of $N-1$. Two special cases (azimuthal and radial vector beams) of cylindrical vector beams are widely used for super-resolution imaging and lithography because of their unique focusing performance, which will be demonstrated in section 4.

$$U = \tilde{A}_{LN} e^{i(N\alpha)} |L\rangle + \tilde{A}_{RM} e^{i(-N\alpha)} |R\rangle \tag{3}$$

Based on the relationship among the FPS, HOPS, and HyOPS [i.e., Eqs. (1) – (3)], a unity design framework can be proposed to generate arbitrary vector vortex beams on HOPS and HyOPS via an all-dielectric metasurface. However, no focusing phase is included in Eq. (1). A hyperbolic focusing phase profile is needed to obtain arbitrary focused vector vortex beams [Eq. (4)] should be imparted to the LCP and RCP components in Eq. (1) [16].

$$\Phi(\rho, f) = \frac{2\pi}{\lambda}(f - \sqrt{f^2 + \rho^2}) \tag{4}$$

$$U(\rho, \alpha) = e^{i[\Phi(\rho) + (\frac{N+M}{2})\alpha]} \{\tilde{A}_{LN} e^{i\left(\frac{N-M}{2}\alpha\right)} |L\rangle + \tilde{A}_{RM} e^{i\left(\frac{M-N}{2}\alpha\right)} |R\rangle\} \tag{5}$$

In Eq. (4), ρ is the radius of the light beam's cross-section. Introducing Eq. (4) to Eq. (1), arbitrary focused vector vortex beams can be expressed as Eq. (5), which indicates that the critical function of the dielectric metasurface would be to impart the polarization-independent phase profile of $\Phi(\rho) + (\frac{N+M}{2})\alpha$ and polarization-dependent phase profile of $\pm(\frac{N-M}{2}\alpha)$ onto an incoming scalar LP beam. To clarify the unified design framework via Eq. (5), sections S1 and S2 in supporting material derived the working mechanism of a dielectric metasurface and provided a general design flow, respectively.

3. Dielectric metasurface for generating arbitrary PS beams

3.1 Metasurface design

As discussed in Section 2, the metasurface needs to impart a propagation phase profile Ψ^{PP} [Eq. (6)] and a geometry phase profile Ψ^{GP} [Eq. (7)] to the transmitted light beam. Based on the

meta-atom library built up in supporting material Section S2, the metasurface can be designed following a general flow as shown in Fig. 2(a).

$$\Psi^{PP}(\rho,\alpha) = \Phi(\rho,f) + (\frac{N+M}{2})\alpha \tag{6}$$

$$\Psi^{GP}(\rho,\alpha) = \pm(\frac{N-M}{2}\alpha) \tag{7}$$

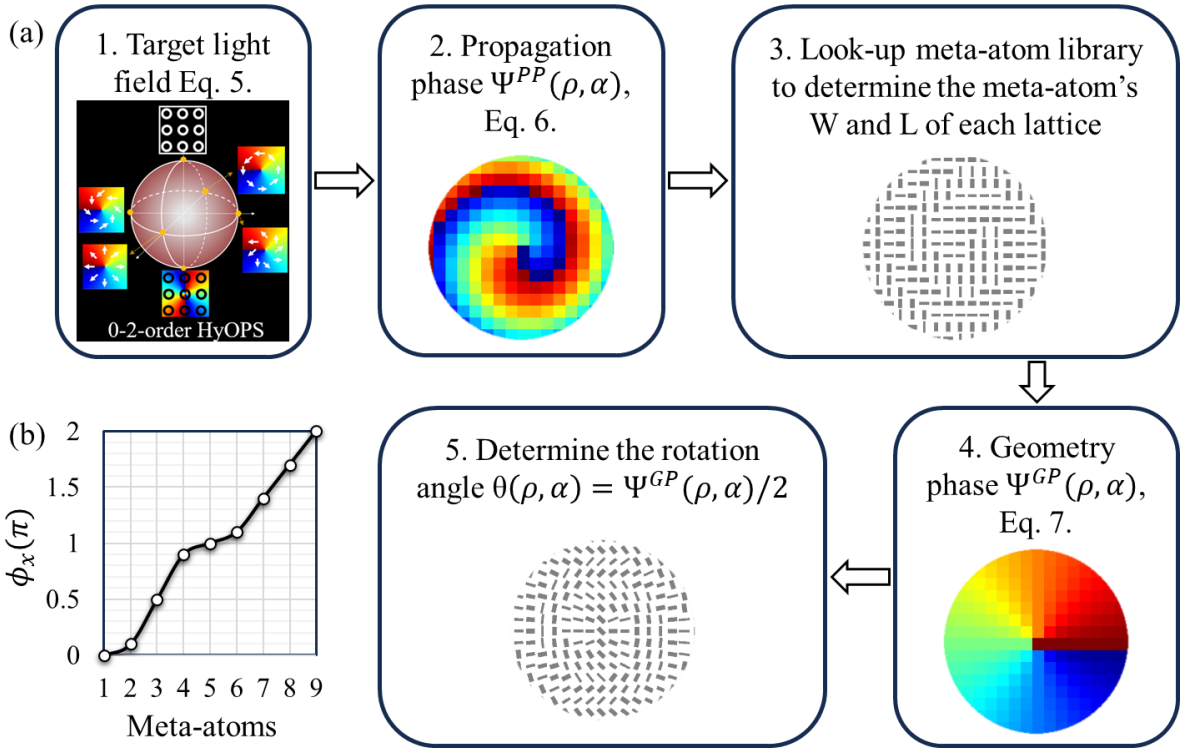

Fig. 2 Design flow (a) and meta-atom's library (b) of the dielectric metasurface for generating HOPS and HyOPS beams.

Taking the metasurface of generating arbitrary focused vector vortex beams on a HyOPS ($M = 0$, $N = 2$, NA = 0.89) as an example, Fig. 2(a) demonstrates the metasurface design flow in detail. Starting from the digitalisation of the target propagation phase $\Psi^{PP}(\rho,\alpha)$, we can first determine the meta-atom's dimension (W, L) at each lattice by looking up the meta-atoms library [Fig. 2(b)]. Next, the required geometry phase profile [Eq. (7)] and the rotation angle $\theta(\rho,\alpha) = \Psi^{GP}(\rho,\alpha)/2$

at each lattice can be determined. As a result, the rotation angle of the meta-atom array owns a distribution of $\theta(\rho,\alpha) = (N-M)\alpha/4$.

3.2 Manipulating the transmitted light over the whole PS surface.

A set of QWP and HWP are adopted to manipulate the transmitted light over the whole PS surface to achieve arbitrary vector vortex beams on a target HOPS or HyOPS [Fig. 3(a)]. An LP light beam (E_γ in Fig. 3, the polarisation direction γ) passing through the QWP and HWP can be described as U_0 [Eq. (8)] based on the Jones matrix.

$$U_0 = \begin{bmatrix} cos\,(2\chi) & sin(2\chi) \\ sin\,(2\chi) & -cos(2\chi) \end{bmatrix} \begin{bmatrix} 1 & 0 \\ 0 & i \end{bmatrix} \begin{bmatrix} \cos(\gamma) \\ \sin(\gamma) \end{bmatrix} \tag{8}$$

$$\begin{cases} \tilde{A}_{LN} = \frac{1}{\sqrt{2}}\,[cos(\gamma) + sin(\gamma)]e^{i(2\chi)} \\ \tilde{A}_{RM} = \frac{1}{\sqrt{2}}\,[cos(\gamma) - sin(\gamma)]e^{i(-2\chi)} \end{cases} \tag{9}$$

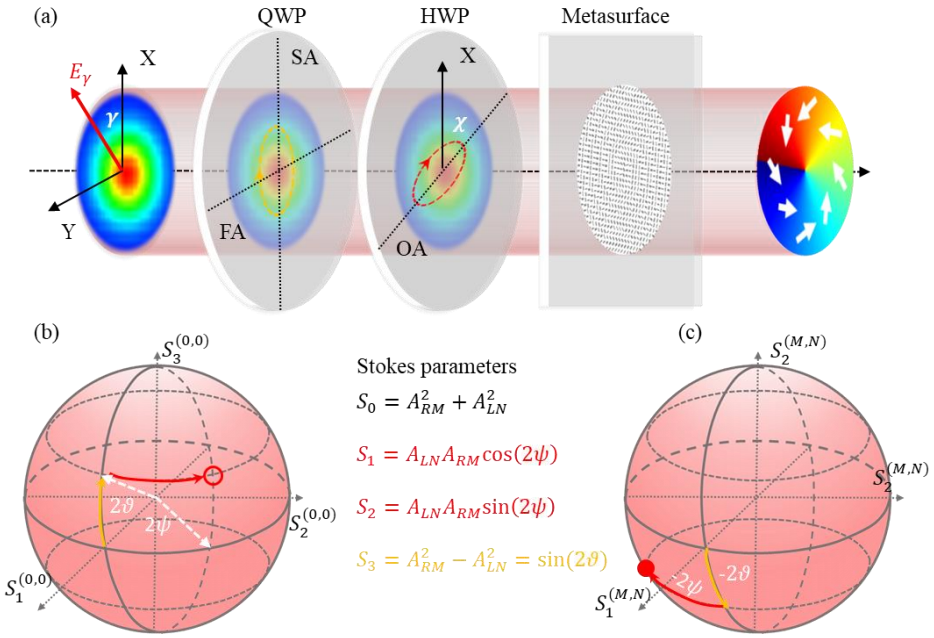

Fig. 3 (a) Scheme of generating arbitrary vector vortex beams on a target HOPS or HyOPS, (b) the circular point represents a scalar beam having a position angle $(2\vartheta, 2\psi)$, (c) the solid red point is the transmitted light beam's position $(-2\vartheta, -2\psi)$ on a HOPS/HyOPS.

To determine the polarisation U_0 (i.e., the polarization angles 2ϑ and 2ψ on an FPS), the complex amplitudes $\tilde{A}_{LN}$ and $\tilde{A}_{RM}$ [Eq. (9) as well as in Eq. (2)] of the LCP and RCP components in U_0 need to be obtained at first. Substituting $\tilde{A}_{LN}$ and $\tilde{A}_{RM}$ into the definition of Stokes parameters, we can obtain the position angles (2ϑ and 2ψ in Fig. 3) [Eq. (10)].

$$\begin{cases} 2\psi = -4\chi \\ 2\vartheta = -2\gamma \end{cases} \tag{10}$$

In Eq. (10), as well as the Stokes parameters, 2ψ denotes the phase difference between the RCP and LCP components. As both χ and γ angles can be continuously tuned from 0 to 2π, arbitrary values of 2ψ and 2ϑ (i.e., $\tilde{A}_{LN}$ and $\tilde{A}_{RM}$) can be obtained. Therefore, a set of HWP and QWP can achieve arbitrary beams represented by an FPS.

Substituting Eqs. (6), (7), and (9) into Eq. (S5), the light beam passing through the metasurface sample can be obtained as Eq. (11), which demonstrates arbitrary vector vortex beams on a specific HOPS and HyOPS. As shown in Figs. 3(b) and 3(c), after passing through the metasurface, the light beam's position on a HOPS and HyOPS would be opposite to its position on the FPS because the LCP (RCP) component is converted be RCP (LCP) by the metasurface [Eqs. (9) and (11)].

$$\begin{bmatrix} E_x^o \\ E_y^o \end{bmatrix} = e^{i\left[\Phi(\rho)+\left(\frac{N+M}{2}\right)\alpha\right]}\{\frac{1}{\sqrt{2}}\,[cos(\gamma)-sin(\gamma)]e^{i(-2\chi)}e^{i\left(\frac{N-M}{2}\alpha\right)}|L\rangle + \cdots$$

$$\cdots\frac{1}{\sqrt{2}}\,[cos(\gamma)+sin(\gamma)]e^{i(2\chi)}e^{i\left(\frac{M-N}{2}\alpha\right)}|R\rangle\} \tag{11}$$

Specifically, when $\gamma = 0$ (i.e., the polarisation direction of the incoming light is along the SA of the QWP), 2ϑ equal to zeros [Eq. (10)] as well. It means that, for $\gamma = 0$, Eq. (11) represents the vector beams on the equator of the HOPS and HyOPS. Introducing $\gamma = 0$ to the Eq. (8), the outgoing light beam $U_0(\gamma = 0) = \begin{bmatrix} \cos(2\chi) \\ \sin(2\chi) \end{bmatrix}$ which is LP and has a polarisation direction $\beta = 2\chi$. Substituting $\beta = 2\chi$, $\theta(\rho, \alpha) = (N - M)\alpha/4$, and Eq. (6) into Eq. (S9), we can obtain the light

beam transmitted from the metasurface [Eq. (12)]. Eq. (12) demonstrates that the vector beams represented by the HOPS and HyOPS' equator are a set of cylindrical vector vortex beams with an order of $(N-M)/2$ and a topological charge of $(N+M)/2$. For example, when $N = 2$, $M = 0$, the equator represents a set of cylindrical vector vortex beams with an order of 1 and a topological charge of 1, as shown in Figs. 1(c) and 3(a). While Eq. (12) agrees with Eq. (11), based on a linear polarisation basis, Eq. (12) gives a clearer and simpler description of the cylindrical vector vortex beams represented by the equator.

$$\begin{bmatrix} E_x^o \\ E_y^o \end{bmatrix}_{\gamma=0} = e^{i\left[\Phi(\rho)+\left(\frac{N+M}{2}\right)\alpha\right]} \begin{bmatrix} \cos\left[\frac{(N-M)\alpha}{2} - 2\chi\right] \\ sin\left[\frac{(N-M)\alpha}{2} - 2\chi\right] \end{bmatrix} \tag{12}$$

We have derived the unified design framework and generation mechanism of arbitrary vector beams on a HOPS/HyOPS. Specifically, based on the linear polarisation basis, we give a quantitative value of the cylindrical vector vortex beams represented by a HOPS/HyOPS' equator. Four proof-of-concept experiments are operated in section 4, where four metasurface samples are used with customised functions (i.e., design parameters). The design parameters and target function of the four samples are summarised in Table 1.

Table 1 Parameters and target of metasurface samples

Number of samples	Design parameters	Target
1	$M = 5, N = -5, \Phi(\rho) = 0$	Non-focused 5th-order HOPS beams
2	$M = 5, N = -5, f = 300\mu m$	Focused 5th-order HOPS beams (NA=0.89)
3	$M = 0, N = 2, f = 1mm$	Focused 0-2 order HyOPS beams (NA=0.89)
4	$M = 0, N = 1, f = 1mm$	Focused 0-1 order HyOPS beams (NA=0.89)

4. Proof-of-concept experiments

4.1 Sample 1 for generating non-focused 5th-order HOPS beams.

The metasurface sample 1 is first designed by setting $M = 5, N = -5, \Phi(\rho) = 0$ to generate arbitrary non-focused 5th-order HOPS beams. The intensity distribution of the transmitted light beam is

theoretically calculated based on Eq. (11) and illustrated in Fig. 4(a). The position angles (2ϑ, 2ψ) in Fig. 4(a) are obtained based on the Eq. (10) and the parameters (γ, χ) adopted for Eq. (11). Considering the orthogonality of the X- and Y-components in the transmitted light and the symmetry of the X- and Y-component's intensity, Fig. 4(a) only depicts the near-field of the X-component in the transmitted light beam. As shown in Fig. 4(a), the near field distribution of the X-component becomes a gear-like pattern from an almost uniform pattern by manipulating the 2ϑ from $\pm\frac{\pi}{2}$ to 0. (i.e., the transmitted light beam $\begin{bmatrix} E_x^o \\ E_y^o \end{bmatrix}$ is manipulated from the two poles to the equator).

In the experiment, the transmitted light beam $\begin{bmatrix} E_x^o \\ E_y^o \end{bmatrix}$ is collected via a customised microscope where sample 1 is illuminated by a collimated 1550nm laser beam. To obtain the near-field distribution of the X-component, the microscope is focused on sample 1 (Z = 0), and a polariser is placed in front of the camera to select the X-component in the transmitted light beam. Fig. 4(b) shows the experiment result where the near-field of the X-component is tuned to be clearly gear-like pattern from an almost uniform pattern by manipulating the 2γ (i.e., -2ϑ)from $-\frac{\pi}{2}$ to 0.

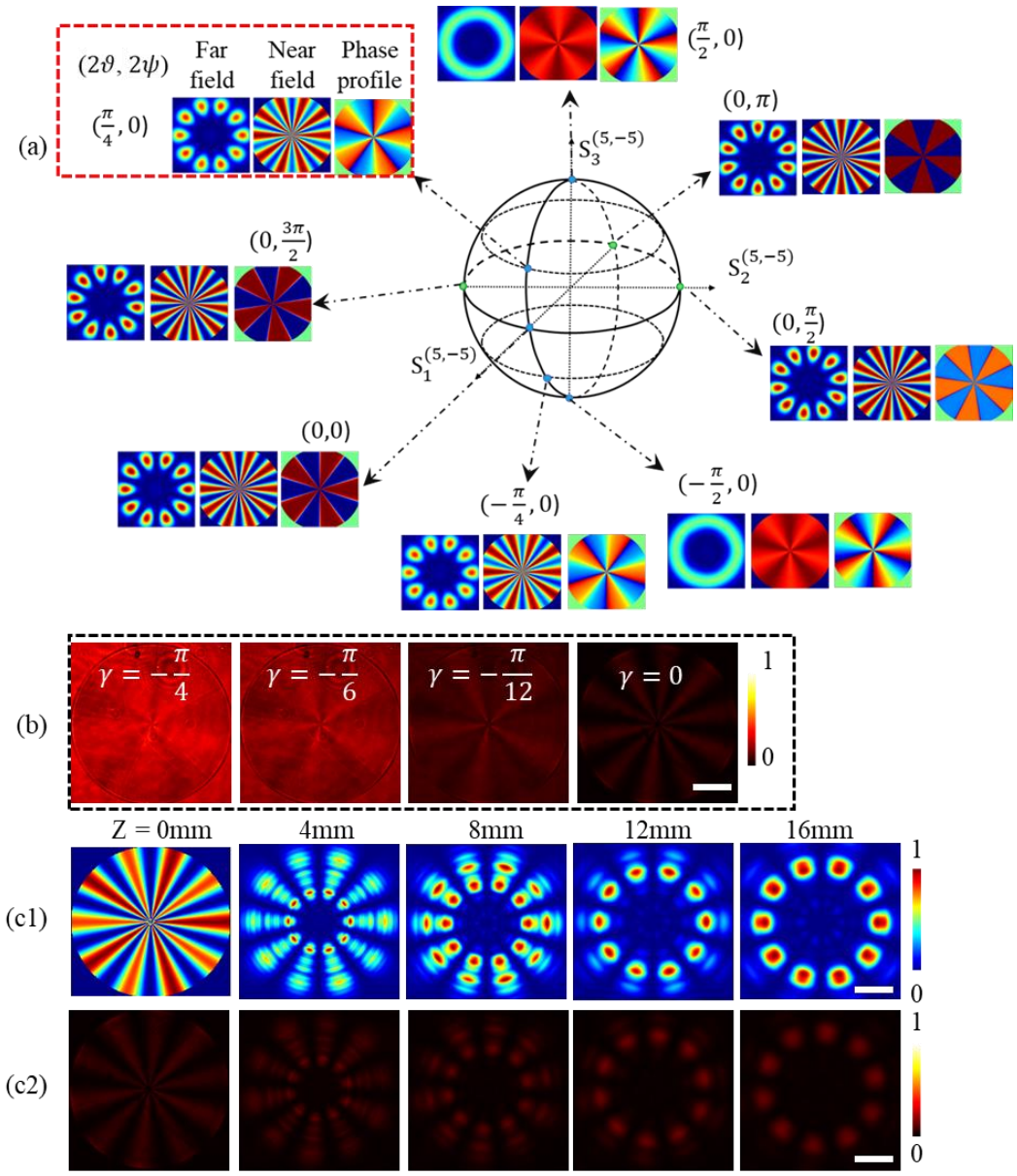

Fig. 4 (a) Simulated far-field, near-field, and phase profile distribution of the X-component in the transmitted light beams over the target 5th-order HOPS by manipulating the position angles $(2\vartheta, 2\psi)$, (b) measured near-field distribution of the X-component, (c1) and (c2) are the simulated and experimental results of the X-component's propagation evolution from the metasurface (Z=0mm) to Z = 16mm. Scale bars: $130\mu m$.

Based on the Fourier transformation of the near field, the far field of the X-component is obtained and shown in Fig. 4(a) as well. The distribution of the near field and far field of the transmitted light beam is quite different, as shown in Fig. 4(a). Therefore, it is meaningful to figure

out how the transmitted light beam evolutes from the near field pattern (Z = 0) to the far field pattern. Keeping $\gamma = 0$ ($2\vartheta = 0$), the intensity evolution with the propagation distance Z is theoretically obtained via angular spectrum theory [27] and measured in the experiment. The theoretical and experimental results are shown in Figs. 4(c1) and 4(c2), respectively. Our experimental results coincide well with the theoretical results. From both numerical and experimental results, the gear-like near field (Z = 0mm) gradually converges to the expected far-field pattern with multiple lobes at around Z = 12mm, and then the far-field pattern becomes divergent (Z > 12mm).

4.2 Sample 2 for generating tightly focused 5th-order HOPS beams

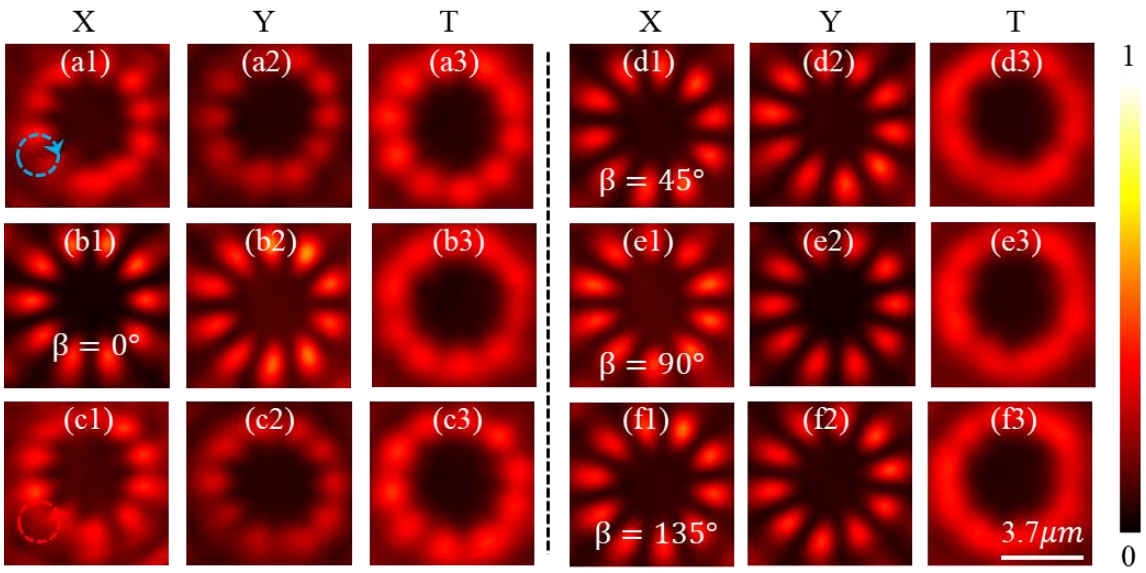

Fig. 5 Experiment results: controlled generation of tightly-focused 5th-order HOPS beams along its longitude line (a) – (c) and along its equator (d) – (f). The 1st and 4th columns are the X-components in the total focal fields T (3rd and 6th columns), and the 2nd and 5th columns are the Y-components.

To obtain the tightly focused 5th-order HOPS beams via the metasurface, the metasurface sample 2, with a diameter of 1.2mm, is designed by setting M = 5, N = -5, and *f* equals 300 μm. The target

NA of sample 2 is 0.89. The tightly focused far field (Fig. 5) is measured at the focal plane of sample 2.

Figure 5 demonstrates the controlled generation of tightly focused 5th-order HOPS beams along its longitude line and equator by tuning the angles (γ, χ). It could be seen that the far field of X- and Y-components is orthogonal to each, and the total fields are donut-shape over the whole 5th-order HOPS. From the first 3 columns in Fig. 5, the X- and Y-components spread to be donut-shaped [Figs. 5(a) and 5(c)] from 10 lobes [Fig. 5(b)] with manipulating the 2γ (i.e., -2ϑ) from 0 to $\pm\pi/2$. Keeping $\gamma = 0$, We observed that the 10 lobes in X- and Y-components rotated by the angle of HWP (i.e., $\beta = 2\chi$) [Figs. 5(b), and 5(d) – 5(f)]. The far-field distributions (Fig. 5) measured in the focal plane of sample 2 match well with the theoretically obtained far-field distribution [Fig. 4(a)].

To show the tightly-focusing property of the 5th-order HOPS beams, the size of each lobe in the Figs. 5(b), and 5(d) – 5(f) is quantitatively evaluated. Each lobe has a tiny lateral full width of half maximum (FWHM) of 828nm, which is 22% smaller than the diffraction limitation (1062nm, $0.61\lambda/NA$), which indicates that the tightly focused HOPS beams can be used for super-resolution imaging and photolithography.

4.3 Sample 3 for generating tightly focused 0-2 order HyOPS beams

We studied the metasurface sample 3 with a diameter of 4mm in simulation and experiment for generating arbitrary focused beams on the 0-2 order HyOPS. As shown in Fig. 1(c), from the northern pole to the southern pole along a latitude line, the TC gradually increases to 2 from 0. The beams on its equator are the 1st-order CVVBs with a TC of 1 [Eq. (12)]. It is firstly verified that the outgoing beams from the metasurface can be tuned from a scalar RCP (LG00, TC, $\ell = 0$) to a CVVB (TC, $\ell = 1$) and to a scalar LCP (LG00, TC, $\ell = 2$) with the incident laser beam being

tuned from a scalar LCP to an LP and an RCP beam in simulation (first three columns in Fig. 6). With rotating polarisation direction of the incident LP beam, arbitrary 1st-order CVVBs (TC, $\ell = 1$) is generated via this metasurface (last three columns in Fig. 6).

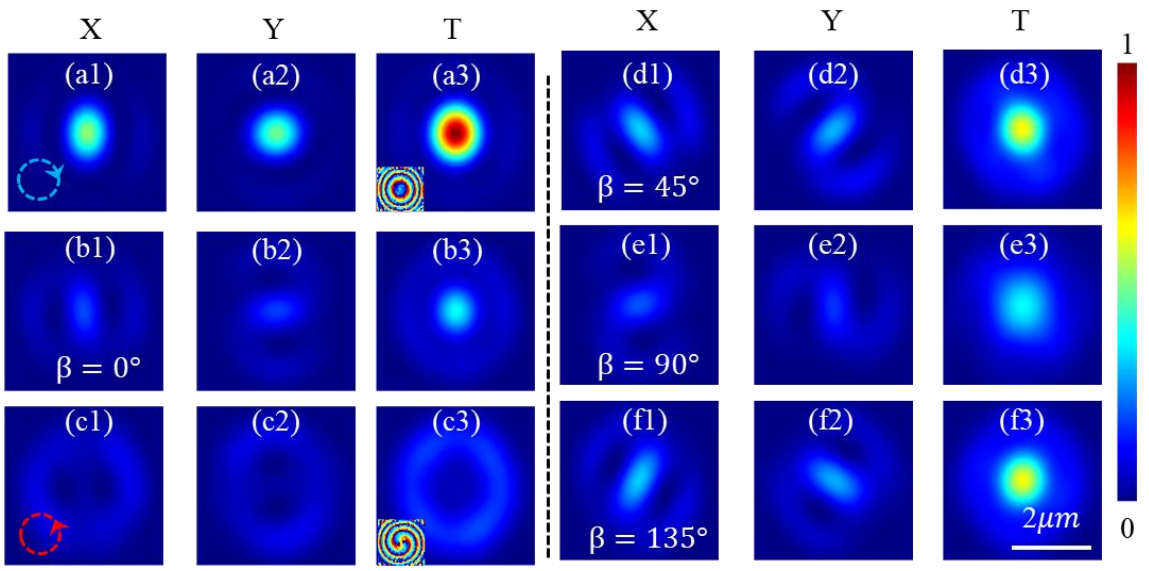

Fig. 6 Simulation results: controlled generation of 0-2 order HyOPS beams along its longitude line (a) – (c) and along its equator (d) – (f). The 1st and 4th columns are the X-components in the total focal fields T (3rd and 6th columns), and the 2nd and 5th columns are the Y-components.

The LG00 focal point is measured to obtain the metasurface's NA under the LCP beam illumination. The full width of half maximum (FWHM) of the LG00 focal point is measured to be 1060nm [Fig. 7(c1)], demonstrating that the fabricated metasurface has a NA of 0.89. As the incident beam's polarisation state changes from LCP to RCP, the focal point is tuned from a diffraction-limited LG00 spot [Fig. 7(a)] to an LG02 doughnut [Fig. 7(c)] along the 0-2 order HyOPS latitude line. We can see the intensity in the focal plane gradually spreads from the central area to the doughnut ring [Figs. 7(a)-7(c)] with the incident laser beam's polarisation being tuned from LCP to RCP by rotating a QWP.

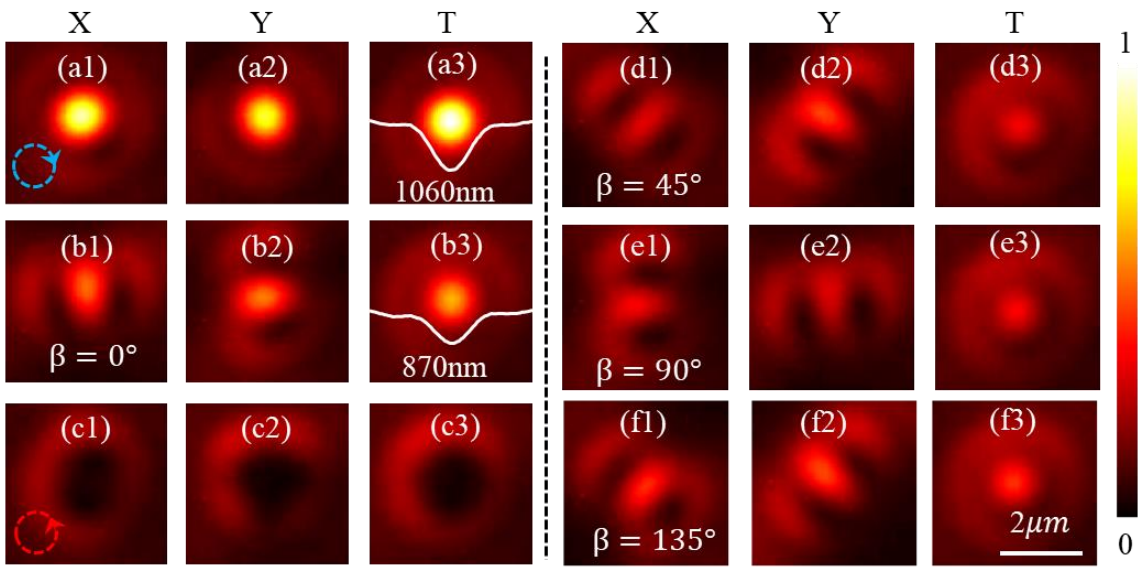

Fig. 7 Experiment results: controlled generation of 0-2 order HyOPS beams along its longitude line (a) – (c) and along its equator (d) – (f). The 1st and 4th columns are the X-components in the total focal fields T (3rd and 6th columns), and the 2nd and 5th columns are the Y-components.

As predicted by Eq. (12) and simulation results in Fig. 6, we can experimentally generate arbitrary 1st-order CVVBs by manipulating the illumination light beam's polarisation direction β via rotating the HWP [Figs. 7(b) and 7(d)-2(f)]. For $\beta = 0$, an azimuthal vector vortex beam (a special case of the CVVBs) is generated and is tightly focused. As a result, a focal point (FWHM = 870nm), which is smaller by 18% than the diffraction limitation (1062nm, $0.61\lambda/NA$) is obtained [Fig. 7(b)]. We also observed that the focal point's size goes up and its intensity goes down with the polarisation direction changing from X-polarized ($\beta = 0°$) beam to Y-polarized beam ($\beta = 90°$). Furthermore, it is measured that the 8-shaped intensity distribution of the X-components (1st and 3rd columns in Fig. 7) and Y-components rotates with the polarisation direction β [Figs. 7(b1) and 7(d1)-7(f1)].

4.4 Sample 4 for generating tightly focused 0-1 order HyOPS beams

The order (1) and topological charge (1) of the CVVBs generated by the 0-2 order HyOPS are integer values, and a super-resolution focal point beyond diffraction-limitation is obtained in both simulation and experiment. It is theoretically reported that there is a distinct focusing property between the CVVBs with integer order/topological charge and fractional order/topological charge. We designed and fabricated sample 4 with a diameter of 4mm to study the difference in the experiment. Sample 4 is studied in simulation (Fig. 8) and experiment (Fig. 9), according to Eqs. (11), the topological charge carried by all vector vortex beams on the 0-1 order HyOPS is fractional. Based on Eq. (12), The CVVBs represented by the 0-1 order HyOPS' equator have an order of 0.5 and a topological charge of 0.5.

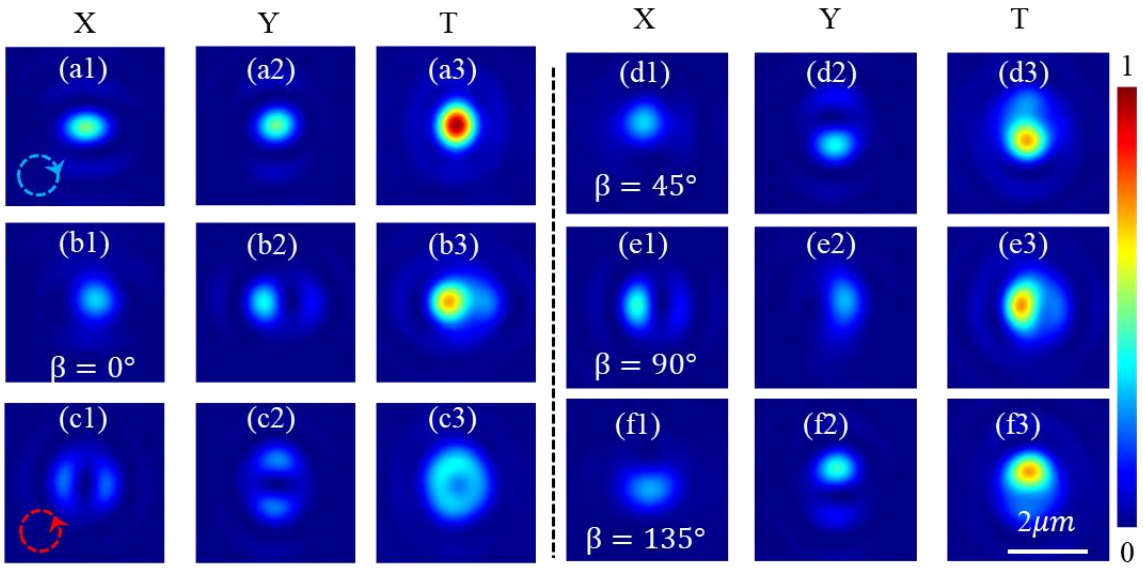

Fig. 8 Simulation results: controlled generation of 0-1 order HyOPS beams along its longitude line (a) – (c) and along its equator (d) – (f). The 1st and 4th columns are the X-components in the total focal fields T (3rd and 6th columns), and the 2nd and 5th columns are the Y-components.

We studied the tunability of the topological charge of the transmitted light beam by manipulating the illumination light beam's polarisation state. With the illumination light beam tuned from LCP to RCP, the transmitted light beam is tuned from a diffraction-limited Gaussian spot [FWHM = 1060nm, Figs. 8(a3) and 9(a3)] to an LG01donut [Figs. 8(c3) and 9(c3)]. Because the topological

charge (1) carried by the southern pole of 0-1 order HyOPS is smaller than that (2) of the 0-2 order HyOPS, we observed that the radius of the central holes shown in Figs. 8(c3) and 9(c3) is smaller than that in Figs. 6(c3) and 7(c3).

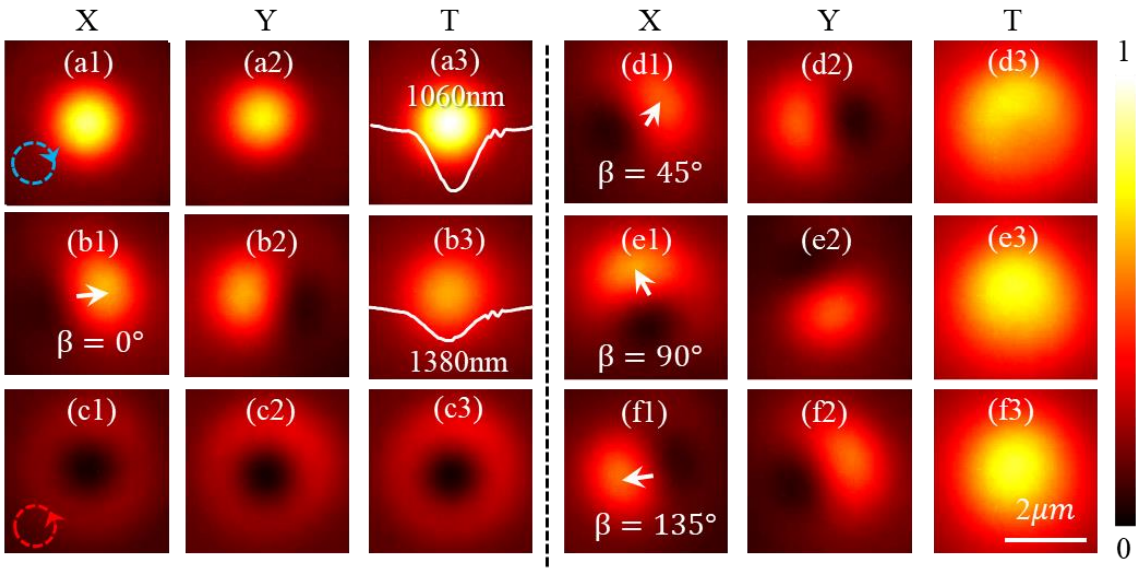

Fig. 9 Experiment results: controlled generation of 0-1 order HyOPS beams along its longitude line (a) – (c) and along its equator (d) – (f). The 1st and 4th columns are the X-components in the total focal fields T (3rd and 6th columns), and the 2nd and 5th columns are the Y-components.

Comparing the data in sections 4.3 and 4.4, we can see a clear difference in the intensity evolution along the longitude line of the 0-1 order and 0-2 order HyOPS from the northern to southern poles. While the light energy spreads from a Gaussian solid point to a doughnut and keeps rotational symmetric for the 0-2 order HyOPS (section 4.3), the light intensity maximum is offset from the optical axis and intensity distribution becomes non-symmetric around the optical axis for the 0-1 order HyOPS (section 4.4). Moreover, a non-axial zero point appears in the focal field of arbitrary vector vortex beams on the 0-1-order HyOPS, which arises from the superposition of the fractional vortex phase carried by the LCP and RCP components [Eq. (11)].

When sample 4 is illuminated by an LP light beam, the uniaxial symmetric property is distinct in the focal plane [Fig. 9(b)]. As a result, the FWHM of the total field [Fig. 9(b3)] is 1380nm and larger than the diffraction limitation. With changing the linear polarisation direction β, the non-axial maximum intensity [arrows in Figs. 9] and null intensity in X- and Y-components rotate around the optical axis. These experiment results in Fig. 9 match well with the simulation results in Fig. 8 and the reported theoretical results in reference [36]. As far as we know, the tightly focusing properties of fractional VVBs and CVVBs are experimentally reported for the first time, highlighting our unified design framework's merit.

5. Conclusion and discussion

A general design framework of the single-layer dielectric metasurface is proposed to generate arbitrary non-focused/focused vector vortex beams on HOPS/HyOPS. The design framework is proposed by deriving the phase modulation mechanism of the single-layer dielectric metasurface via Jones-matrix and theoretically analysing the connection between the HOPS and HyOPS. The controlled generation mechanism is illustrated based on the T-matrix method. Based on an orthogonal linear polarisation basis, the simultaneous modulation of local polarisation direction and phase is obtained for the first time to analyse the controlled generation of the cylindrical vector vortex beams on the HOPS/HyOPS' equator. As a result, it is figured out that the vector order and topological charge of the cylindrical vector vortex beams represented by the equator of M-N-order HyOPS are $(N-M)/2$ and $(N+M)/2$, respectively. When $M=-N$, the vector order and topological charge are N and zeros, which means that the beams represented by the equator of the N^{th}-order HOPS are N^{th}-order cylindrical vector beams without vortex phase.

We operated four detailed proof-of-concept experiments to show the merit of our unified design framework. At first, the non-focused and tightly-focused (NA = 0.89) 5th-order HOPS

beams are generated in both simulation and experiments to demonstrate HOPS beams' propagation and focusing properties. Then, the tightly focused (NA = 0.89) 0-2 order and 0-1 order HyOPS beams are respectively generated via another two metasurface samples. In the experiment, we observed the super-resolution focusing performance of the 1st-order cylindrical vector vortex (topological charge is 1) beams on the 0-2 order HyOPS' equator and the different focusing properties of integer-order (0-2 order HyOPS equator beams) and fractional-order cylindrical vector vortex (0-1 order HyOPS equator beams) beams.

Based on the proposed unique design framework for generating arbitrary HOPS/HyOPS beams with tailored focusing profile, we conceive this research could not only boost the metasurface's applications in multi-mode imaging, laser communication, structured optical tweezers, and the HOPS/HyOPS-beams-based metrology systems. It's well known that the imaging modes of an infinite-corrected microscope relies on the point spread function as well as the focal field's distribution of the objective lens, a multi-mode imaging system can be achieved by adopting a metasurface (e.g., the samples 2, 3, 4) with a polarization-controlled focal field. The HOPS/HyOPS beams have been regarded as the high-potential candidates for achieving high-capacity laser communication and structured optical tweezers, and the highly focusing of HOPS/HyOPS beams is of vital importance. Conventionally, the HOPS/HyOPS beams are firstly generated by a metasurface or spatial light modulator and then focused by a high-NA lens for the structured optical tweezers. In contrast, we demonstrated a more compact solution of these applications by integrating the generation and high-focusing of HOPS/HyOPS beams into one single-layer metasurface via the proposed design framework. In addition, the metasurface-based compact generation of focused HOPS/HyOPS beams paves the way of developing miniaturized and hand-held precision metrology system. More important, the researchers on developing HOPS/HyOPS

beams-based application systems have a little of knowledge of designing and fabricating a metasurface. We conceive this paper would reduce the barriers for them to generate arbitrary unfocused/focused HOPS/HyOPS beams via a single-layer dielectric metasurface.

Disclosures

The authors declare no conflicts of interest.

Code, Data, and Materials Availability

All data in support of the findings of this paper are available within the article or as supplementary material.

Acknowledgements and funding

PhD studentship from the Chinese Scholarship Council is acknowledged. This work is supported by the UK's Engineering and Physical Sciences Research Council (project number EP/V000624/1, EP/X03495X/1, EP/X041166/1 and EP/T02643X/1), and supported by the Royal Society (project number RG\R2\232531).

References

1. Chao He, Yijie Shen, and Andrew Forbes, “Towards higher-dimensional structured light,” *Light. Sci. Appl.* **11**, 205(2022).
2. Isaac Nape, Keshaan Singh, Asher Klug, et al., "Revealing the invariance of vectorial structured light in complex media," *Nat. Photon.* **16**, 538-546 (2022).
3. Min Liu, Yunze Lei, Lan Yu, et al., "Super-resolution optical microscopy using cylindrical vector beams" *Nanophotonics* **11**(15), 3395-3420(2022).
4. E. otte, C.Denz, "Optical trapping gets structure: Structured light for advanced optical manipulation," *Appl. Phys. Rev.* **7**, 041308 (2020).

5. Gabrielius Kontenis, Darius Gailevičius, Noé Jiménez, and Kęstutis Staliunas, "Optical Drills by Dynamic High-Order Bessel Beam Mixing," *Phys. Rev. Applied* **17**, 034059(2022).
6. Qiwen Zhan, "Cylindrical vector beams: from mathematical concepts to applications," *Adv. Opt. Photon.* **1**, 1-57 (2009).
7. Giovanni Milione, H. I. Sztul, D. A. Nolan, and R. R. Alfano, "Higher-Order Poincaré Sphere, Stokes Parameters, and the Angular Momentum of Light," *Phys. Rev. Lett.* **107**, 053601 (2011).
8. Yi, Xunong, et al. "Hybrid-order Poincaré sphere." *Physical Review A* **91**(2), 023801 (2015).
9. Lin, Di, et al. "Reconfigurable structured light generation in a multicore fibre amplifier." *Nature communications* **11**(1), 3986 (2020).
10. Yijie Shen, et al. "SU(2) Poincaré sphere: A generalized representation for multidimensional structured light." *Physical Review A* **102**, 031501 (2020).
11. Yijie Shen, et al. "Optical vortices 30 years on: OAM manipulation from topological charge to multiple singularities," *Light. Sci. Appl.* **8**, 90(2019).
12. Yijie Shen, et al. "Structured ray-wave vector vortex beams in multiple degrees of freedom from a laser," *Optica.* **7**(7), 820 (2020).
13. Zhensong Wan, et al. "Ultra-Degree-of-Freedom Structured Light for Ultracapacity Information Carriers," *ACS Photonics.* **10**, 2149 (2023).
14. Nanfang Yu et al., Light Propagation with Phase Discontinuities: Generalized Laws of Reflection and Refraction. *Science* **334**,333-337(2011).
15. Chen, Mu Ku, et al. "Principles, functions, and applications of optical meta-lens." *Advanced Optical Materials* **9(4)**, 2001414 (2021).
16. Chen, Wei Ting, Alexander Y. Zhu, and Federico Capasso. "Flat optics with dispersion-engineered metasurfaces." *Nature Reviews Materials* **5(8)**, 604-620 (2020).
17. Kamali, Seyedeh Mahsa, et al. "A review of dielectric optical metasurfaces for wavefront control." *Nanophotonics* **7(6)**, 1041-1068 (2018).

18. Dorrah, A.H., Rubin, N.A., Zaidi, A. et al. "Metasurface optics for on-demand polarization transformations along the optical path." *Nat. Photonics* **15**, 287–296 (2021).
19. Ren, H., Fang, X., Jang, J. et al. "Complex-amplitude metasurface-based orbital angular momentum holography in momentum space." *Nat. Nanotechnol.* **15**, 948–955 (2020).
20. Xie, YY., Ni, PN., Wang, QH. et al. "Metasurface-integrated vertical cavity surface-emitting lasers for programmable directional lasing emissions." *Nat. Nanotechnol.* **15**, 125–130 (2020).
21. Wen, Dandan, and Kenneth B. Crozier. "Metasurfaces 2.0: Laser-integrated and with vector field control." *APL Photonics* **6(8)** (2021).
22. Sroor, Hend, et al. "Generation of arbitrary higher order Poincaré beams from a visible metasurface laser." *Laser Resonators, Microresonators, and Beam Control XXII*. Vol. 11266. SPIE (2020).
23. Xiangyu Zeng, et al. "Arbitrary manipulations of focused higher-order Poincaré beams by a Fresnel zone metasurface with alternate binary geometric and propagation phases," *Photon. Res.* **10**, 1117-1126 (2022)
24. D. Wen, et al. "Broadband Multichannel Cylindrical Vector Beam Generation by a Single Metasurface." *Laser Photonics Rev* **16**, 2200206 (2022).
25. Bao, Yanjun, Jincheng Ni, and Cheng-Wei Qiu. "A minimalist single-layer metasurface for arbitrary and full control of vector vortex beams." *Advanced Materials* **32(6)**, 1905659 (2020).
26. Wang, S., Deng, ZL., Wang, Y., et al. "Arbitrary polarization conversion dichroism metasurfaces for all-in-one full Poincaré sphere polarizers. " *Light Sci Appl* **10**, 24 (2021).
27. Li, Guixin, et al. "Spin-enabled plasmonic metasurfaces for manipulating orbital angular momentum of light." *Nano letters* **13(9)**, 4148-4151 (2013).
28. Li, Hui, et al. "Polarization Detection of Terahertz Waves using All-Silicon Metasurfaces with Tightly Focusing Behavior." *Laser & Photonics Reviews*, 2300428 (2023).
29. Ji, Jitao, et al. "Metasurface-Enabled On-Chip Manipulation of Higher-Order Poincaré Sphere Beams." *Nano Letters* **23(7)**, 2750-2757 (2023).

30. Wang, Shuai, et al. "Metasurface-Based Solid Poincaré Sphere Polarizer." *Physical Review Letters* **130(12)**, 123801 (2023).
31. Robert C. Devlin, et al. "Arbitrary spin-to–orbital angular momentum conversion of light." *Science* **358**,896-901(2017).
32. Liu, Junmin, et al. "Generation of arbitrary cylindrical vector vortex beams with cross-polarized modulation." *Results in Physics* **19**, 103455 (2020).
33. Yang, Jiaqi, Tommi K. Hakala, and Ari T. Friberg. "Generation of arbitrary vector Bessel beams on higher-order Poincaré spheres with an all-dielectric metasurface." *Physical Review A* **106(2)**, 023520 (2022).
34. Cao, Guangtao, et al. "Infrared metasurface-enabled compact polarization nanodevices." *Materials Today* **50**, 499-515 (2021).
35. Feng, Z., Tang, T., Wu, T. et al. "Perfecting and extending the near-infrared imaging window. " *Light Sci Appl* **10**, 197 (2021)
36. Miao, Yu, et al. "Tight-focusing properties of propagable fractional-order vector vortex beams." *JOSA B* **40(5)**, 1113-1120 (2023).